Multiband Magnetless Isolators and Circulators With Reconfigurable Bandpass Filtering Capabilities

Dakotah Simpson, *Member, IEEE*, and Dimitra Psychogiou, *Senior Member, IEEE*

***Abstract*— This article reports on the RF design and practical validation of new classes of magnetless multiband isolators and circulators with reconfigurable bandpass filtering capabilities. They are based on transversal frequency-selective signal paths shaped by frequency-tunable and spatiotemporally modulated resonators. Each path creates a passband that can be independently controlled in terms of frequency and direction of propagation. Thus, the overall network may exhibit 1-to-*K* frequency-reconfigurable non-reciprocal passbands. The operating principles and schematic of the magnetless and reconfigurable filtering isolator concept are first demonstrated through circuit-based simulations of two- and three-path transversal filtering networks (i.e., two- and three-band networks). The independent modulation parameters of the bands are determined through detailed parametric analyses. Next, the concept is extended to the design of magnetless, multiband filtering circulators. The operating and design principles of the circulator are expounded through a circuit schematic and an ideally simulated dual-band example. For practical demonstration purposes, three lumped-element (LE) prototypes, two isolators, and one circulator, shaped by two or three RF signal paths (i.e., two and three passbands), were implemented at very high frequency (VHF) band. They exhibited a maximum in-band isolation (IS) up to 50 dB. Moreover, a frequency tuning of up to 1.22:1 and change of directionality are achieved.**

***Index Terms*— Bandpass filter (BPF), circulator, dual band, isolator, lumped-element (LE) filter, multiband, non-reciprocal filter, non-reciprocity, spatiotemporal modulation (STM), tunable filter.**

I. Introduction

NON-RECIPROCAL components, such as isolators and circulators, are fundamental elements of many important microwave communication, radar, and instrumentation systems due to their ability to protect sensitive RF devices from high-power reflected signals and to separate the transmit and receive operation of full-duplex RF systems. Historically, their operation is enabled by incorporating magnetically biased ferromagnetic materials within their volume. However, due to the need for external magnetic biasing, magnetic-based circulators/isolators are large in size and cannot be integrated with other IC-based front-end circuitry.

Recent research efforts are attempting to overcome this size limitation by the following: 1) incorporating transistors or operational amplifiers in the RF circuit [1], [2]; 2) developing magnetic materials with inherent magnetization—i.e., self-biased [3]; 3) breaking the time-reversal symmetry through staggered commutation in *N*-path filters [4]; or 4) utilizing spatiotemporal modulation (STM) [5], [6], [7], [8], [9], [10], [11]. STM is an effective method to achieve non-reciprocity without bulky magnetic biasing. It has been extensively used in optical devices and most recently in the design of non-reciprocal bandpass filters (BPFs). The BPFs in [7], [8], [9], [10], and [11] have adequately made use of STM to achieve non-reciprocity in lumped-element (LE) and microstrip-type configurations. However, these concepts have only been demonstrated for single-band operation without mention of how to extend them to additional passbands or how to achieve tunability within the RF circuit, which is central to modern RF front ends. Furthermore, it is crucial to be able to control their resonant frequency, mode of operation (reciprocal and non-reciprocal), and number of bands with the purpose of functionalizing multiconfigurable RF systems.

STM has also been used in the creation of magnetless circulators. For example, the circulator presented in [12] uses a wye topology where each branch of the circulator is created by the cascade of two series *LC* resonators. The resonators in each branch are modulated with the same signal, and there is a phase progression between each branch and the next. Nevertheless, this article only shows simulated results and a maximum isolation (IS) of 32 dB. Another example is shown in [13] where a similar modulation scheme is used except only one resonator per branch is modulated. A microstrip prototype is presented, but the circulator shows a low IS of up to 27 dB. Other examples of magnetless circulators are shown in [6], [14], [15], and [16]. There main drawbacks include a moderate IS of up to 28 dB in [14] and [15], only simulated examples in [16], and a high insertion loss (IL) of 9 dB in [6]. Furthermore, all of them are single-band designs without being extendable to multiband topologies. Besides, only one demonstrates frequency tuning with a low tuning range of 1.06:1 [15].

In consideration of the aforementioned limitations in the field of magnetless isolators and circulators, this article presents, for the first time, a new class of multiband magnetless isolators and circulators with reconfigurable bandpass filtering

Manuscript received 13 May 2022; revised 18 September 2022; accepted 15 October 2022. This work was supported in part by the National Science Foundation under Grant ECCS-1941315. *(Corresponding author: Dakotah Simpson.)*

Dakotah Simpson is with the Department of Electrical, Computer, and Energy Engineering, University of Colorado Boulder, Boulder, CO 80309 USA (e-mail: dakotah.simpson@colorado.edu).

Dimitra Psychogiou is with the Department of Electrical and Electronic Engineering, University College Cork, Cork, T12 K8AF Ireland, and also with the Tyndall National Institute, Cork, T12 R5CP Ireland (e-mail: dpsychogiou@ucc.ie).

Color versions of one or more figures in this article are available at https://doi.org/10.1109/TMTT.2022.3218114.

Digital Object Identifier 10.1109/TMTT.2022.3218114

capabilities. Their passbands can be independently tuned in terms of center frequency, directionality, and number of active bands in the direction of propagation. They are based on multiple in-parallel paths of BPFs that comprise frequency-tunable and time-modulated resonators. Non-reciprocity is achieved by breaking the time-reversal symmetry through STM. By altering the dc biasing of the resonators and the STM parameters, the passbands of the components can be independently tuned in terms of frequency, number, and direction of propagation.

The rest of this manuscript is organized as follows. Section II first reports on the operational and design principles of the reconfigurable filtering isolator and then details the filtering circulator through circuit schematics and circuit-simulated transmission and reflection responses. To practically verify the proposed multiband magnetless isolator and circulator approach, the RF design, realization, and experimental validation of three LE prototypes, including two isolators and one circulator, are presented in Section III. Moreover, their performances are discussed in relation to the state of the art. Finally, a summary of the main contributions of this work is provided in Section IV.

II. Theoretical Background

A. Magnetless RF Codesigned Multiband Isolator/Filter

The schematic and conceptual power transmission, reflection, and IS responses of the proposed magnetless, multiband filtering isolator are shown in Fig. 1. The devised multiband isolator concept is based on a parallel-path network that comprises K Nth-order bandpass filtering paths, each contributing a passband to the transfer function. Although identical in operation, the paths operate independently of one another and at different frequencies and have unique sets of parameters that define them. The distinct coupling elements and resonators in each path are responsible for this phenomenon. Path 1 is responsible for defining the lower frequency passband, Path 2 determines the next frequency passband, and Path K defines the highest frequency passband.

Each path is made of N resonators whose resonant frequencies are controlled by dc and ac biasing signals applied to their varactor-based capacitors. The dc biasing sets the nominal capacitance and the center frequency of the passband. Furthermore, the time-dependent ac biasing modulates the capacitance in time and gives rise to the directionality of the RF signal propagation throughout the filter path.

The parameters of the ac signals (modulation voltage: V_M, modulation frequency: f_M, and phase: Φ) must be properly selected through optimization or through parametric analyses for non-reciprocity to be achieved. Moreover, a progressive phase shift, $\Delta\Phi$, between the ac signals of the modulated resonators needs to be applied, as depicted in Fig. 1(a), to impart the directionality in the filter path. Both Φ and V_M control the IS level and transfer function of each path. With the appropriate selection of the modulation parameters, a K-band transfer function is present in the forward direction (S_{21}) and RF signal cancellation in the reverse one (S_{12}) as demonstrated in the conceptual transfer function of Fig. 1(b). By varying the dc bias on the path's varactor diodes, the affected passband's center frequency can be tuned as is conceptually shown in

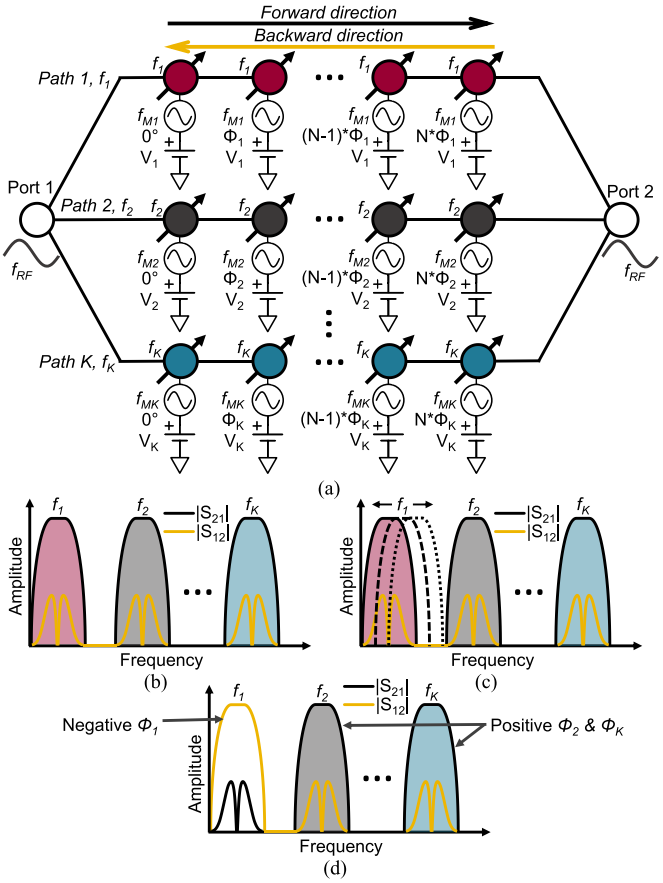

Fig. 1. Concept of the magnetless isolator with reconfigurable bandpass filtering capabilities. (a) Schematic of a K-band Nth-order BPF; colored circles: frequency-tunable resonators, white circles: RF input and RF output, and black lines: impedance inverters. (b) Conceptual response of a K-band transfer function. (c) Conceptual response showing center frequency tuning of the lower passband. (d) Conceptual response showing reconfigurable directionality (i.e., transmission or cancellation of the RF signal) in the lower passband by reversing the sign of the phase progression between the resonators.

Fig. 1(c). Finally, Fig. 1(d) demonstrates the reconfigurability of the direction of propagation in one of the passbands (i.e., reconfigurability of number of passbands in each direction of propagation) in order to obtain a bandstop-type filtering response for the first band in the forward direction. This can be done to reject unwanted interfering or jamming signals that may appear within the first band's frequency range. It is accomplished by reversing the sign of the progressive phase shift on the resonators of the path. Specifically, the progressive phase shift decreases from 0 to $N \times -\Phi$ from port 1 to port 2 instead of increases from 0 to $N \times \Phi$.

To better elaborate on the operating principles of the proposed multiband filtering isolator, Fig. 2 shows a circuit-equivalent representation of a third-order dual-band (i.e., $N = 3$ and $K = 2$) BPF example alongside the ac and dc biasing scheme that allows for the modulation of the resonators' capacitances. The static impedance inverters have been implemented with the first-order high-pass pi-type LE networks that consist of one series capacitor and two shunt inductors. After combining in-parallel components where possible, the resulting components of this transformation are L_1, L_{2x},

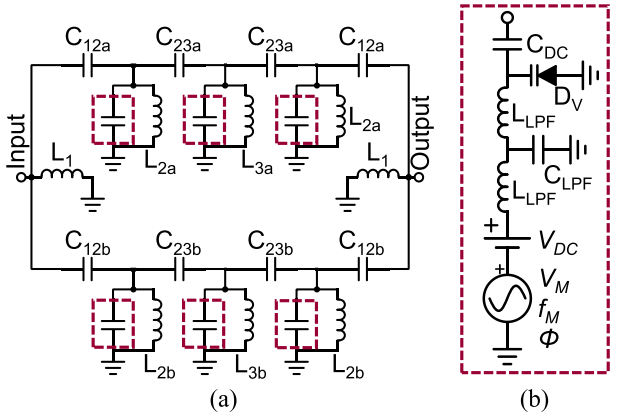

Fig. 2. Circuit schematic of a reconfigurable dual-band filtering isolator for $N = 3$ and $K = 2$. (a) Overall architecture. (b) Detailed schematic of the dc biasing and ac modulation network used to modulate the capacitance of each of the resonators.

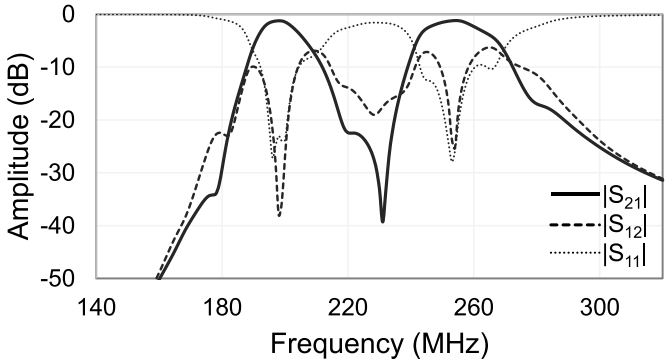

Fig. 3. Ideally simulated power transmission and reflection responses of the dual-band isolator in Fig. 2.

L_{3x}, C_{12x}, and C_{23x}, where $x = a$ and b for the lower and upper passbands, respectively. The resonators have been conventionally realized as parallel LC resonators, where the capacitors are replaced with the network shown in Fig. 2(b). It consists of a varactor diode (D_V) that is biased through a lowpass filter, made of L_{LPF} and C_{LPF}, with a cutoff frequency higher than the modulation frequency but much lower than the RF frequency. A high-valued dc blocking capacitor (C_{dc}) is added to block the dc current from entering other parts of the circuit.

The values of the components are found by first designing a static, reciprocal, parallel-path BPF (e.g., the ones found in [17], [18], [19], [20], [21], and [22]) for the desired center frequencies, bandwidths (BWs), and passband shape (e.g., Butterworth). Alternatively, individual single-band BPFs can be designed and then placed within the same circuit by connecting them to the same input and output ports and readjusting the input and output couplings for impedance matching. After the ideal static design, the capacitors within the resonators are then replaced with dc-biased varactor diodes and biasing circuitry. If distributed-type resonators are used, then they can be loaded with varactor diodes.

It is important to note that the nominal capacitance needs to be within the middle of the range of values achievable by the varactor diode to allow for frequency tuning in both directions. Afterward, the ac modulation parameters (f_M, V_M, and Φ) are obtained through either optimization or parametric analyses with the intent of achieving minimum in-band IL in the forward direction and maximum IS in the reverse direction. The parameters of each path are found in independent optimizations or sweeps.

In order to illustrate the aforementioned design steps, a third-order dual-band filtering isolator was ideally designed using as a basis the schematics in Figs. 1(a) and 2. The bands were designed to exhibit the center frequencies of 200 and 250 MHz and the BWs of 15 MHz (7.5%) and 20 MHz (8%), respectively. The circuit-based simulations were completed using the software package Advanced Design System (ADS) from Keysight. An SMV1413 varactor diode model from Skyworks and ideal LE components were used in the simulations that follow. The varactor diode included loss as given by its data sheet ($R_S = 0.35\ \Omega$), and the other components were lossless. The values of the utilized components in this example are as follows: $L_1 = 67.3$ nH, $L_{2a} = 58.3$ nH, $L_{3a} = 82.1$ nH, $L_{2b} = 37.4$ nH, $L_{3b} = 50.3$ nH, $L_{\text{LPF}} = 350$ nH, $C_{12a} = 3.9$ pF, $C_{23a} = 0.7$ pF, $C_{12b} = 3.3$ pF, $C_{23b} = 0.7$ pF, $C_{\text{dc}} = 82$ pF, and $C_{\text{LPF}} = 82$ pF.

Fig. 3 shows the response of the filter after the optimal ac modulation parameters have been selected. It exhibits the low-minimum in-band IL levels of 1.24 and 1.19 dB and the high maximum directivities of 36.7 and 24.1 dB. The modulation parameters were chosen through a series of variable sweeps shown in Figs. 4 and 5, where the modulation parameters of the lower and upper passbands, respectively, have been swept. D is the directivity and is calculated as the difference between the forward transmission, $|S_{21}|$, and the backward transmission, $|S_{12}|$. The selected values of each parameter have been marked with a dashed line in each plot.

It can be seen that the modulation parameters of one passband do not affect the other passband. As shown in the first column of Figs. 4 and 5, an f_M of about 12.5 MHz leads to a low IL in the forward direction but also a high IS in the reverse direction. Too high modulation frequency results in high IL levels and low directivity. A modulation frequency that is too low decreases the directivity. In the second column, the effects of the modulation voltage, V_M, are shown. The nominal modulation voltage is $\approx$0.15 V_{pp}, because this gives a high directivity with a low IL. It can be observed that lower modulation voltages result in lower IL; however, the directivity decreases too. Higher V_M values lead to a large increase in IL and a narrower BW. Finally, the third column demonstrates how the phase progression between resonators, Φ, affects the filter's response. A phase progression of 60° gives a balance between low IL and high directivity. The IL suffers if the phase progression deviates from 60°, whereas the directivity stays relatively constant within a narrow range around this nominal.

Tuning of the center frequency of each passband is achieved by varying the nominal value of the capacitance via the dc biasing of the varactors. In turn, the modulation voltage must also be adjusted to ensure the capacitance is not

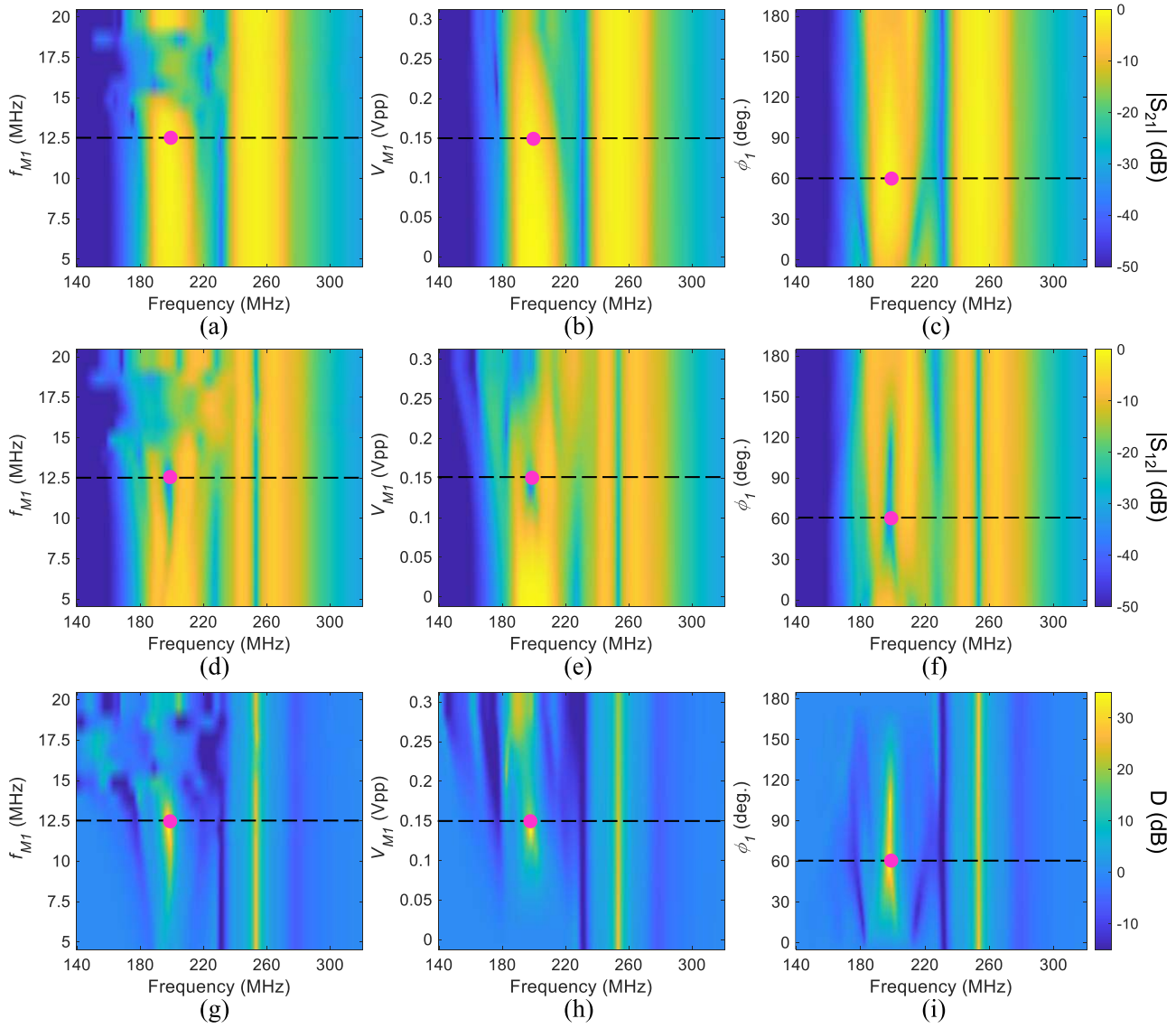

Fig. 4. Simulated power transmission and reflection responses of the dual-band isolator in Fig. 2 as a function of the modulation parameters of signal path #1. The dashed black lines indicate the selected modulation parameter value. The pink dots indicate the center frequency of the lower passband. (a) $|S_{21}|$ as f_{M1} is varied. (b) $|S_{21}|$ as V_{M1} is varied. (c) $|S_{21}|$ as Φ_1 is varied. (d) $|S_{12}|$ as f_{M1} is varied. (e) $|S_{12}|$ as V_{M1} is varied. (f) $|S_{12}|$ as Φ_1 is varied. (g) D as f_{M1} is varied. (h) D as V_{M1} is varied. (i) D as Φ_1 is varied. The modulation parameters of transversal signal path #2 are as follows: $f_{M2} = 12.5$ MHz, $V_{M2} = 0.15$ V_{pp}, and $\Phi_2 = 60°$.

over- or under-modulated given the new dc bias point. The new modulation voltage is obtained by narrowly tuning or optimizing the initial value to find a response with low IL and high IS. In order to thoroughly characterize the tuning capability of the filtering isolator concept, simulated examples of tuning the designed example circuit are shown in Fig. 6(a). Specifically, the first path's (i.e., lower passband's) dc bias voltage is varied from 0 to 0.2 V, while the ac modulation voltage changes from 0.14 to 0.2 V_{pp} to tune the passband in the range of 193–205 MHz. Likewise, the second path's dc bias and modulation voltages are tuned from 0.45 to 0.75 V and 0.13 to 0.2 V_{pp}, respectively, to obtain a frequency tuning of 257–270 MHz. While the passbands were tuned, the modulation frequency and phase progression were unchanged.

Fig. 6(b) shows an example of reconfiguring the direction of propagation of the upper passband by reversing the sign of the phase progression of the modulation signals imparted on the resonators in the second path. Furthermore, this is the method to control the number of active passbands in either direction of propagation. It can be seen that by reconfiguring the upper passband's direction of propagation, only one passband now transmits in the forward direction (S_{21}).

In order to demonstrate the filtering isolator architecture's scalability to higher number of bands, Fig. 7 shows the simulated transmission, reflection, and IS responses of a third-order three-band (i.e., $K = 3$ and $N = 3$) example. The three-band example was designed in the same manner as the dual-band one. First, a static, conventional three-band BPF was designed. The capacitors in the resonators were then replaced with

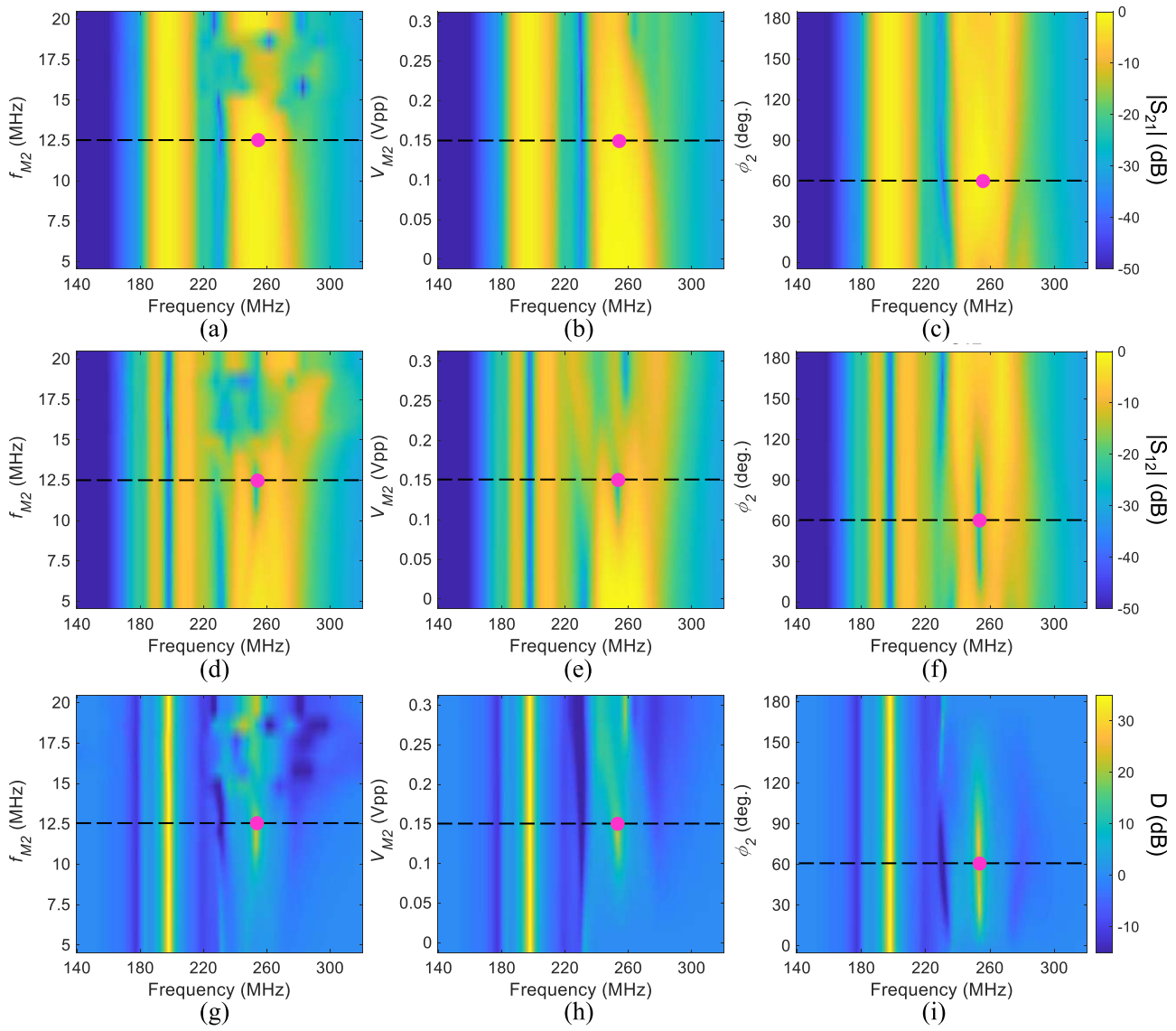

Fig. 5. Simulated power transmission and reflection responses of the dual-band isolator in Fig. 2 as a function of the modulation parameters of signal path #2. The dashed black lines indicate the selected modulation parameter value. The pink dots indicate the center frequency of the upper passband. (a) $|S_{21}|$ as f_{M2} is varied. (b) $|S_{21}|$ as V_{M2} is varied. (c) $|S_{21}|$ as Φ_2 is varied. (d) $|S_{12}|$ as f_{M2} is varied. (e) $|S_{12}|$ as V_{M2} is varied. (f) $|S_{12}|$ as Φ_2 is varied. (g) D as f_{M2} is varied. (h) D as V_{M2} is varied. (i) D as Φ_2 is varied. The modulation parameters of transversal signal path #1 are as follows: $f_{M1} = 12.5$ MHz, $V_{M1} = 0.15$ V_{pp}, and $\Phi_1 = 60°$.

dc-biased varactor diodes. Then, the modulation parameters were found using parametric analyses in the same manner as for the dual-band isolator. As it can be seen in Fig. 7, the passbands can be independently tuned in frequency (lower band in this case), confirming that adding more passbands does not hinder the reconfigurability of the filter.

B. Magnetless RF Codesigned Multiband Circulator/Filter

The conceptual overall and individual branch schematics of the multiband filtering circulator are provided in Fig. 8. As it can be seen, the overall schematic is comprised of three branches, where the composition of a single branch is based on a parallel-path network made of K Nth-order bandpass filtering paths. The output of each branch is connected at a junction in the center of the schematic. Similar to the design of the multiband isolator, each filtering path in the branches contributes one passband to the overall transfer function, and each path can be tuned independently in terms of center frequency and direction of propagation (see Fig. 1) that, in turn, controls the number of active passbands in the direction of propagation. Moreover, each passband has a unique set of parameters that define their performance.

In the presented magnetless, multiband, circulator concept, every resonator in a branch is modulated with the same phase, and the phase is progressed between different branches. In other words, the modulation phase is progressed from branch to branch as opposed to individual resonator to individual resonator in the single-ended isolator case discussed in Section II-A. As it can be seen in Fig. 8, the resonators in the first branch are modulated with a relative phase of 0°,

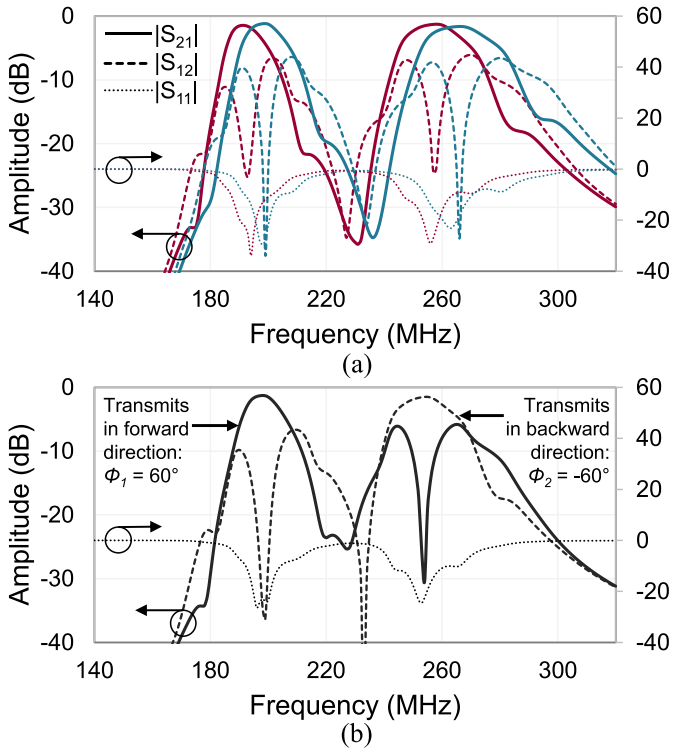

Fig. 6. Simulated power transmission and reflection responses of the dual-band isolator in Fig. 2. (a) Band tuning. (b) Reconfiguration of directionality where the direction of propagation in each band is enabled or disabled by changing the sign of the phase difference between the modulated resonators: $\Phi_1 = 60°$ and $\Phi_2 = -60°$.

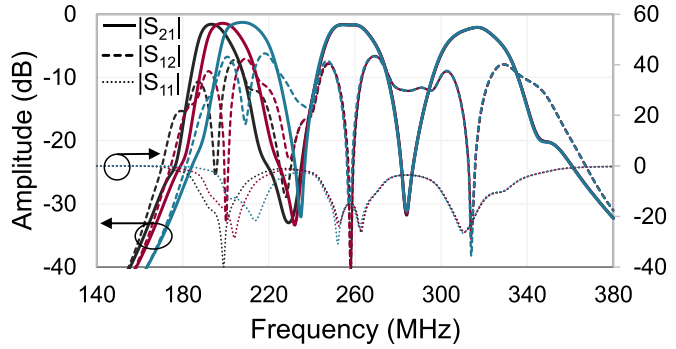

Fig. 7. Simulated power transmission and reflection responses of a three-band, third-order filtering isolator showing band tuning in the lower passband.

and in the second and third branches, the resonators are modulated with the phases of 120° and 240°, respectively. To maintain symmetry between each of the three ports, this phase progression is required.

It should be highlighted that, unlike the design of the isolator in Section II-A, a phase progression between each resonator in a filtering path cannot be used. This is evident when one considers the single-band circulator made of the second-order branches (i.e., $K = 1$ and $N = 2$) shown in Fig. 9. If a phase progression between each resonator is used, the first branch's resonators are modulated with phases 0 and Φ. In order to continue this pattern to the output (port 2 for S_{21}), the second branch's resonators will have the modulation

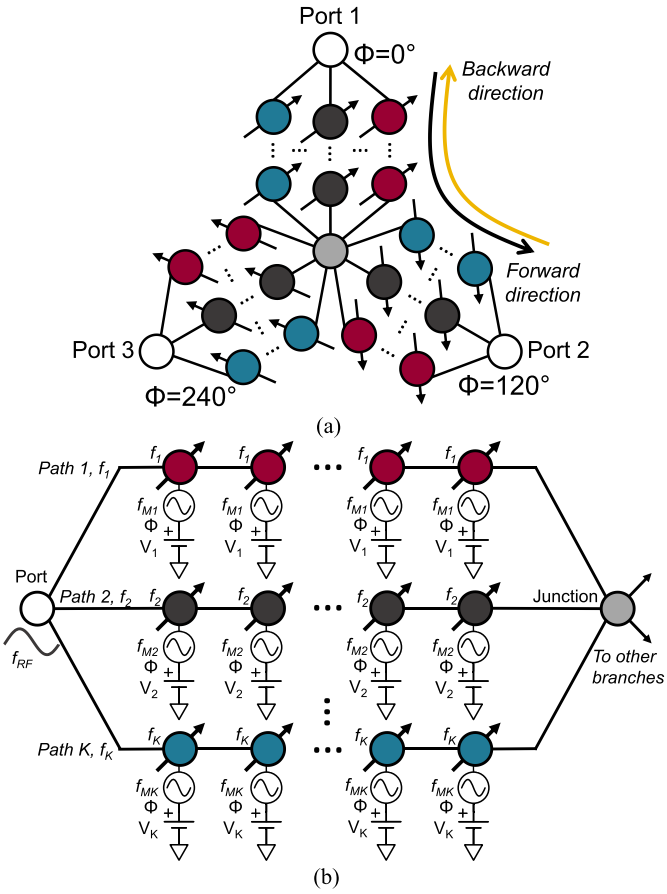

Fig. 8. Schematic of a K-band magnetless circulator that comprises three Nth-order modulated branches; colored circles: frequency-tunable resonators, white circle: RF inputs, gray circle: junction, and black lines: impedance inverters. (a) Overall schematic of the circulator. (b) Schematic and details of one of the three circulator branches.

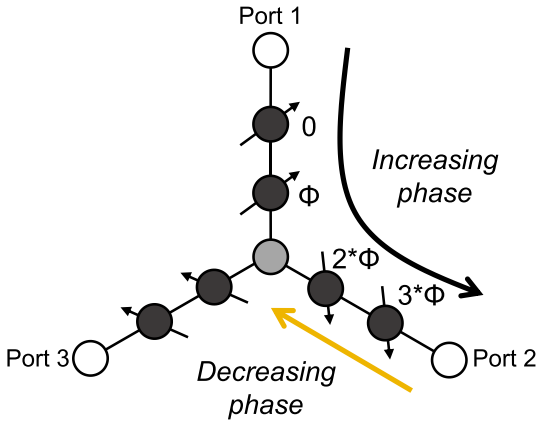

Fig. 9. Schematic of a single-band magnetless circulator that comprises the second-order branches. The diagram demonstrates that a phase progression between individual resonators will not allow simultaneous transmission from port 1 to port 2 and from port 2 to port 3.

phases of $2 \times \Phi$ and $3 \times \Phi$. Thus, the resonator phase progression is 0, Φ, $2 \times \Phi$, and $3 \times \Phi$ from port 1 to port 2. Given these phases, it is impossible to have propagation from port 2 to port 3, since the phase progression is decreasing in this direction (i.e., opposite of the phase progression from

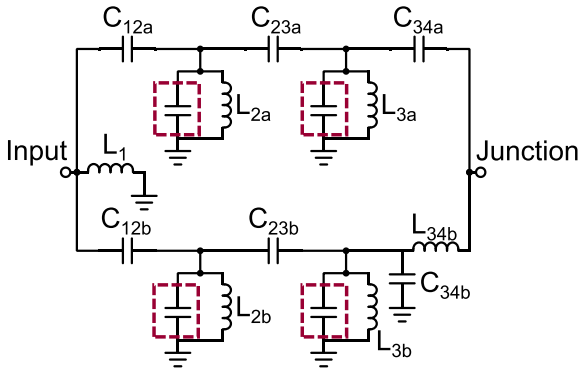

Fig. 10. Circuit schematic of an RF codesigned dual-band filter/circulator branch for $N = 3$ and $K = 2$. The outlined capacitors represent the varactor diode biasing circuitry that is shown in Fig. 2(b).

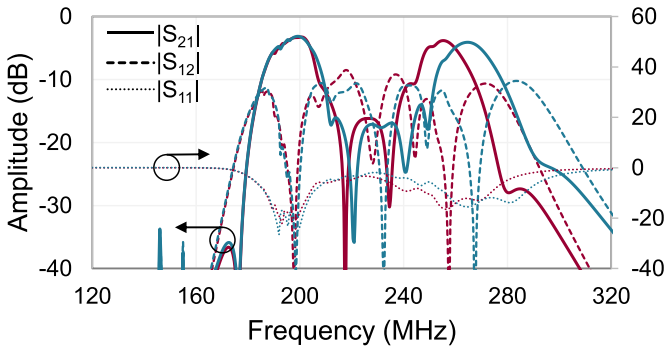

Fig. 11. Simulated power transmission and reflection responses of the example case of a dual-band filtering circulator with $N = 2$ and $K = 2$ showing center frequency tuning of the upper passband.

port 1 to port 2). Therefore, since the resonators of a branch must be used for propagation in both directions (i.e., both to and from the branch's connected port), they need to be modulated identically.

The design of the magnetless circulator follows a similar process to that of the magnetless isolator. First, a static, reciprocal parallel-path BPF is designed for the desired center frequency, BW, and passband shape. The outputs of three of these BPFs are then connected together at a junction without modifying any of their parameters. The resonators' capacitors are then replaced with dc-biased varactor diodes and biasing circuitry. After connecting the branches, the ports become unmatched, because the circuit has three ports and is reciprocal and ideally lossless. Once STM is introduced, the ports will become matched, because the circuit will then be non-reciprocal.

Fig. 10 shows an example circuit schematic of one BPF-based branch for $K = 2$ and $N = 2$. Its varactor-based capacitors, outlined with dashed boxes, utilize the same ac and dc biasing circuitry shown in Fig. 2. After the reciprocal, static design is completed, the modulation parameters are selected in the same manner as in the previous section with the intent of achieving minimum in-band IL in the forward direction and maximum IS in the reverse direction. The parameters of each band can be found independently. With the phases of each resonator determined previously, the other parameters of ac signals (i.e., the modulation voltage and the modulation frequency) still need to be properly selected through optimization or through parametric analyses.

To verify the multiband magnetless circulator concept, Fig. 11 shows the ideally simulated transfer functions of a dual-band circulator with the second-order branches ($K = 2$ and $N = 2$). The circuit in Fig. 10 has been used for the design of the circulator's branches with component values: $L_1 = 50.3$ nH, $L_{2a} = 56.4$ nH, $L_{3a} = 61.2$ nH, $L_{2b} = 35$ nH, $L_{3b} = 60.5$ nH, $L_{34b} = 110.7$ nH, $L_{\text{LPF}} = 350$ nH, $C_{12a} = 5$ pF, $C_{23a} = 1.3$ pF, $C_{34a} = 4.1$ pF, $C_{12b} = 4.6$ pF, $C_{23b} = 1.3$ pF, $C_{34b} = 3.4$ pF, $C_{\text{dc}} = 82$ pF, and $C_{\text{LPF}} = 82$ pF. As it can be seen, each of the bands exhibits high IS in the reverse direction of up to a maximum of 47 dB. Tuning of one band in frequency by adjusting the dc and ac voltage levels applied to the varactor diodes is also shown in Fig. 11, verifying the reconfigurability of the circulator design.

III. Experimental Validation

To validate the proposed magnetless isolator and circulator concepts, three LE prototypes were designed, manufactured, and measured in terms of S-parameters. Specifically, the third-order dual- and three-band isolators ($N = 3$ and $K = 2$ and 3) and a dual-band circulator with the second-order branches ($N = 2$ and $K = 2$) were developed. The dual-band isolator was designed for bands with the center frequencies of 200 and 260 MHz that have the BWs of 14 (7%) and 21 MHz (8.1%), respectively. Furthermore, the bands in the three-band isolator are centered at 200, 260, and 320 MHz with the BWs of 18 MHz (9%), 22 MHz (8.5%), and 25 MHz (7.8%), respectively. The bands of the circulator were designed for the center frequencies of 200 and 260 MHz and the BWs of 15 MHz (7.5%) and 18 MHz (7%).

Their design was performed in ADS and using the initial modulation parameters found in Section II. They were built on a Rogers RO4003C substrate, and SMV1413 varactors from Skyworks were utilized as tuning elements in the circuits' resonators. To provide both the dc and ac biasing, clock-synced arbitrary waveform generators (AWGs) were used. The devices under test (DUTs) are measured using a Keysight N5224A power network analyzer (PNA).

A. Dual-Band Magnetless Isolator/Filter Prototype

A photograph of the manufactured dual-band isolator prototype along with a list of its constituent components and a photograph of the measurement setup are provided in Fig. 12. An RF measured response of the dual-band filtering isolator is compared with an electromagnetic (EM) simulated one in Fig. 13. As it can be seen, non-reciprocity is achieved throughout the two passbands, successfully validating the proposed non-reciprocal multiband concept. The measured center frequencies are 203 and 264 MHz, and the measured BWs are 13 MHz (6.4%) and 21.8 MHz (8.3%). The minimum in-band ILs of the forward transmission ($|S_{21}|$) were measured to be 2.9 and 2.6 dB. The measured IS in the reverse direction ($|S_{12}|$) reaches a maximum of 44.8 and 44.3 dB in the two bands, respectively. Independent tuning of the bands is shown in Fig. 14. The lower band has a tuning range of 198–224 MHz

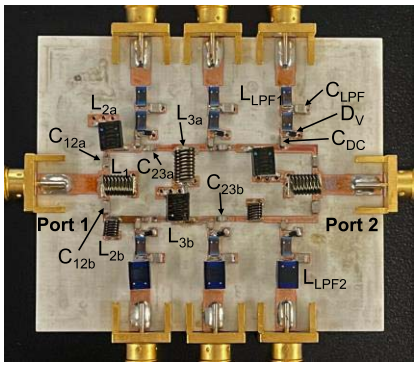

(a)

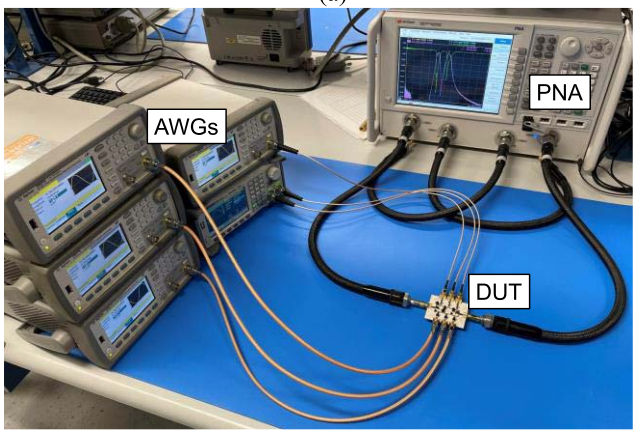

(b)

Fig. 12. (a) Manufactured prototype of the third-order dual-band ($K = 2$ and $N = 3$) isolator. (b) RF-characterization setup.

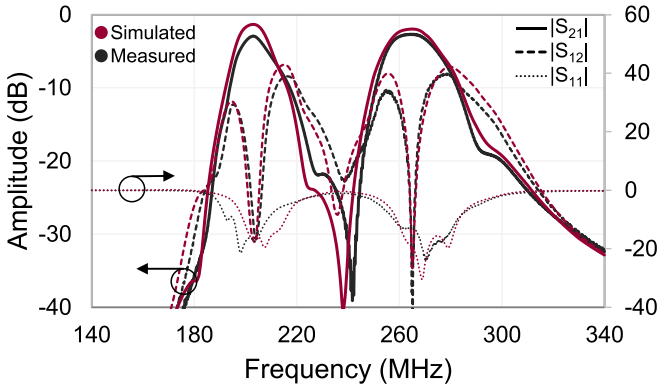

Fig. 13. RF measured and EM simulated power transmission and reflection responses of the manufactured prototype in Fig. 12.

(1.13:1 ratio) in Fig. 14(a), while the upper band can be tuned from 249 to 291 MHz (1.17:1 ratio), as shown in Fig. 14(b). Finally, Fig. 14(c) shows an example of the two passbands transmitting in opposite directions. This is achieved by changing the sign of the phase progression in path 1, so that it increases from port 2 to port 1. As it can be seen, this also changes the number of active bands in the forward direction (S_{21}) from two to one.

B. Three-Band Magnetless Isolator/Filter Prototype

The realized three-band isolator prototype is shown in Fig. 15. For size miniaturization, two of its paths were built on

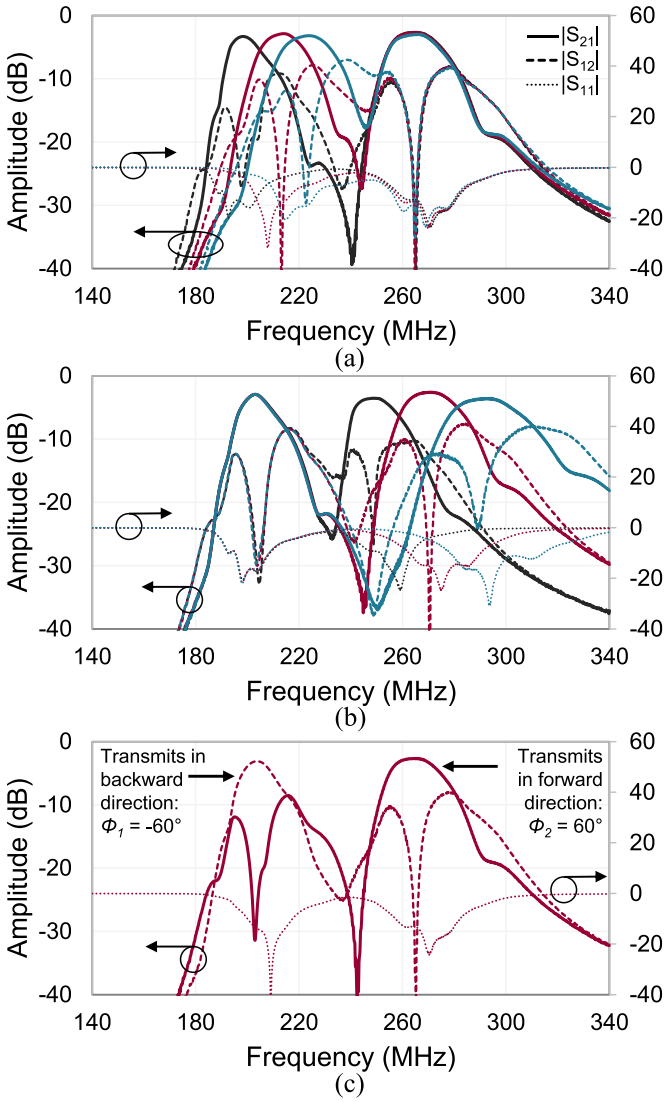

Fig. 14. RF measured power transmission and reflection responses of the manufactured isolator prototype in Fig. 12. (a) Tuning of the lower passband. (b) Tuning of the upper passband. (c) Reconfiguration of directionality in the two passbands by changing the sign of the phase progression in the first path's resonators: $\Phi_1 = -60°$ and $\Phi_2 = 60°$.

the front side of the circuit board, whereas the third path was built on the back side. The path on the back of the board is connected to the input and output ports of the filter and to its biasing networks (located on the front) through 0.8-mm metalized vias. The prototype's RF measured and EM simulated responses are plotted in Fig. 16 and are in a good agreement with each other. The prototype results in three bands with the center frequencies of 202, 257, and 315 MHz. The BWs are measured to be 16.5 MHz (8.2%), 23 MHz (8.9%), and 27.5 MHz (8.7%), respectively. The BPF results in a highly suppressed backward transmission with the maximum in-band IS levels of 30.5, 31.1, and 47.7 dB. Similar to the dual-band prototype, the three-band filter's bands can be independently tuned and can transmit in the reverse direction, as shown in Figs. 17 and 18. In particular, Fig. 17 shows that the bands can tune in the ranges 198–216 MHz (1.1:1), 247–271 MHz (1.1:1), and 302–369 MHz (1.22:1), respectively. Fig. 18

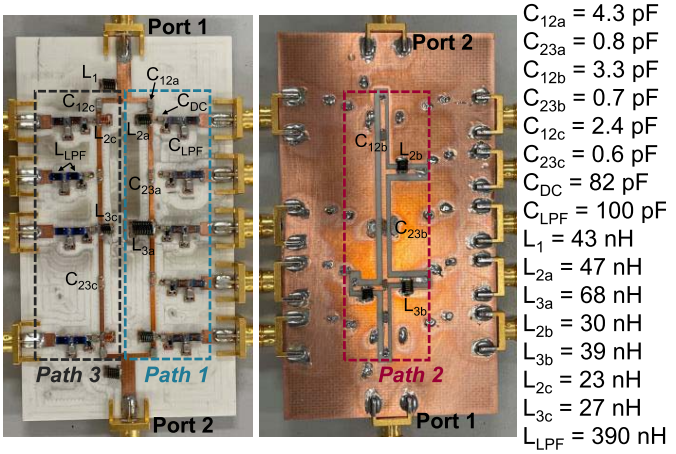

Fig. 15. Manufactured prototype of the third-order three-band ($K = 3$ and $N = 3$) isolator.

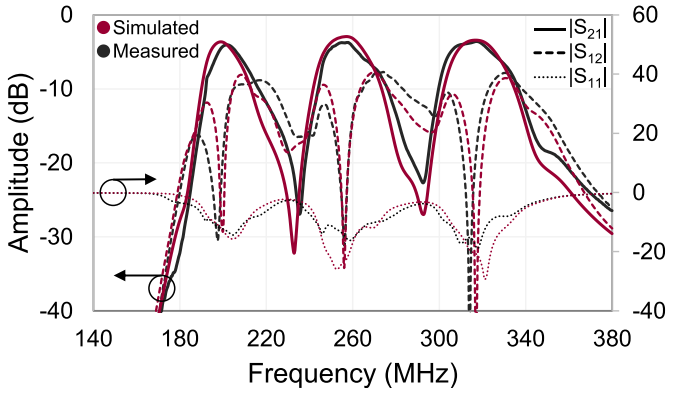

Fig. 16. RF measured and EM simulated power transmission and reflection responses of the manufactured isolator prototype in Fig. 15.

illustrates the filter's responses when one or two of its bands transmit in the reverse direction. This is achieved by changing the sign of the phase progression in paths 1 and 3, so that they increase from port 2 to port 1. By reconfiguring these passbands to transmit in the opposite direction, only one passband is active in the forward direction (S_{21}).

C. Dual-Band Magnetless Circulator/Filter Prototype

The magnetless circulator prototype is shown in Fig. 19. The prototype's RF measured and EM simulated responses are compared in Fig. 20 and appear to be in good agreement, successfully validating the extension of the approach to magnetless circulator designs. Since the circuit is symmetric, $S_{11} = S_{22} = S_{33}$, $S_{12} = S_{31} = S_{23}$, and $S_{21} = S_{13} = S_{32}$. For simplification, only $|S_{11}|$, $|S_{12}|$, and $|S_{21}|$ are shown. The measured center frequencies are 193 and 253 MHz, and the bands' respective BWs are 13.5 MHz (7%) and 16.5 MHz (6.5%). Fig. 21 shows the measured tuning of the bands and the case where one band transmits in the opposite direction of the other (i.e., transmits from port 2 to port 1 instead of the opposite). The lower band can be tuned in the range 185–206 MHz (1.11:1), and the upper band can be tuned from 238 to 270 MHz (1.13:1).

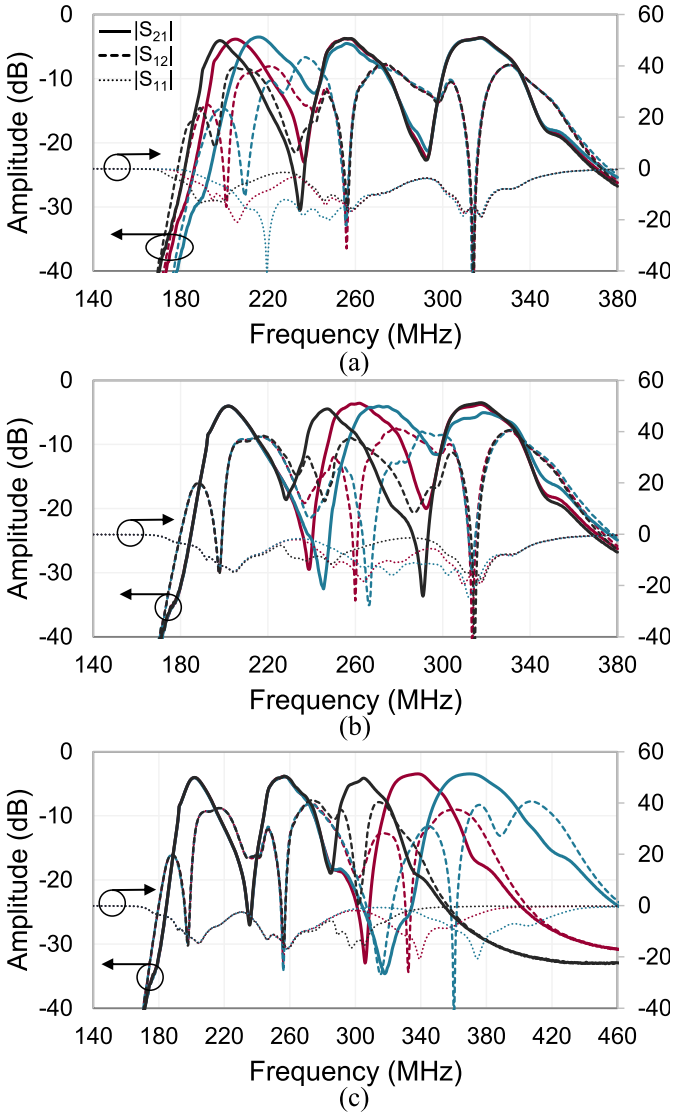

Fig. 17. RF measured power transmission and reflection responses of the manufactured isolator prototype in Fig. 15. (a) Tuning of the lower passband. (b) Tuning of the middle passband. (c) Tuning of the upper passband.

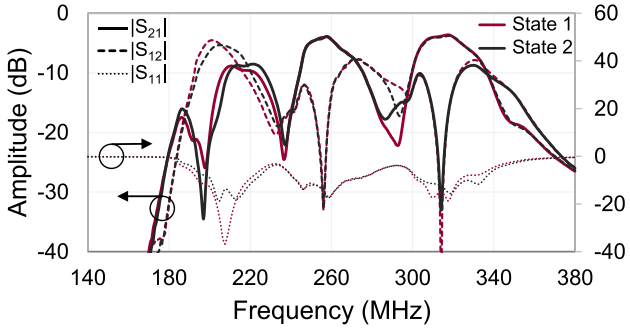

Fig. 18. RF measured power transmission and reflection responses of the manufactured isolator prototype in Fig. 15 showing reconfiguration of directionality. State 1: $\Phi_1 = -60°$, $\Phi_2 = 60°$, and $\Phi_3 = 60°$. State 2: $\Phi_1 = -60°$, $\Phi_2 = 60°$, and $\Phi_3 = -60°$.

D. Comparison With the State of the Art

To demonstrate the potential of the proposed multiband, non-reciprocal isolator, and circulator concepts,

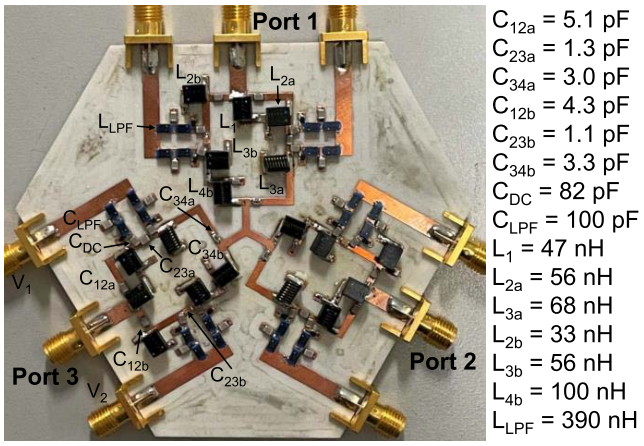

Fig. 19. Manufactured dual-band circulator prototype comprising second-order branches ($N = 2$ and $K = 2$).

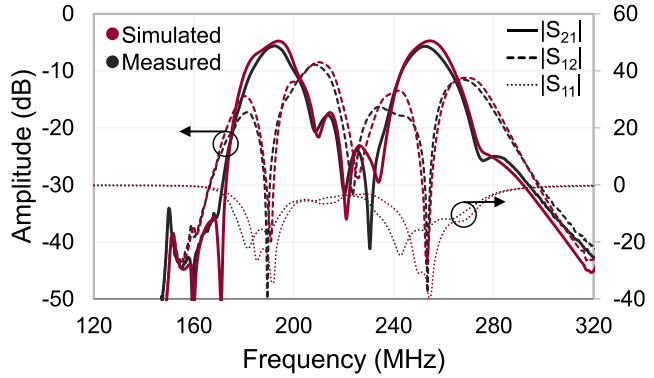

Fig. 20. RF measured and EM simulated power transmission and reflection responses of the manufactured circulator prototype in Fig. 19.

TABLE I
COMPARISON WITH STATE-OF-THE-ART FILTERING MAGNETLESS ISOLATORS

Work	f_{cen}, MHz	BW, MHz (%)	IL, dB	In-band IS, dB	N	T
[7]	186	33 (17.7)	1.5	8-23	3	S
[8]	1020	65 (6.4)	5.5	10-11.7	2	S
[9]	885-1031 (1.17:1)	42 (4.2)	3.9	10-29	3	F
[10]	136-163 (1.2:1)	27.5 (19.2)	3.7	9-52.8	3	F
[11]	270-310 (1.15:1)	15-41.5 (5.2-14.3)	1.7-4.3	6.5-30.9	3	F, BW
This work, dual-band	198-224 (1.13:1), 249-291 (1.17:1)	13 (6.4), 21.8 (8.3)	2.9, 2.6	8.4-44.8, 8-44.3	3, 3	F, D, B
This work, three band	198-216 (1.1:1), 247-271 (1.1:1), 302-369 (1.22:1)	16.5 (8.2), 23 (8.9), 27.5 (8.7)	4.0, 3.7, 3.6	9.4-30.5, 9-36.5, 8.5-49.8	3, 3, 3	F, D, B

IS – Isolation, N – order, T – tunability, S – static, F – frequency, D – direction of propagation, B – number of active bands

Tables I and II compare the prototypes of this article to other state-of-the-art prototypes. As it can be seen in Table I, the proposed filtering isolators are the only multiband and

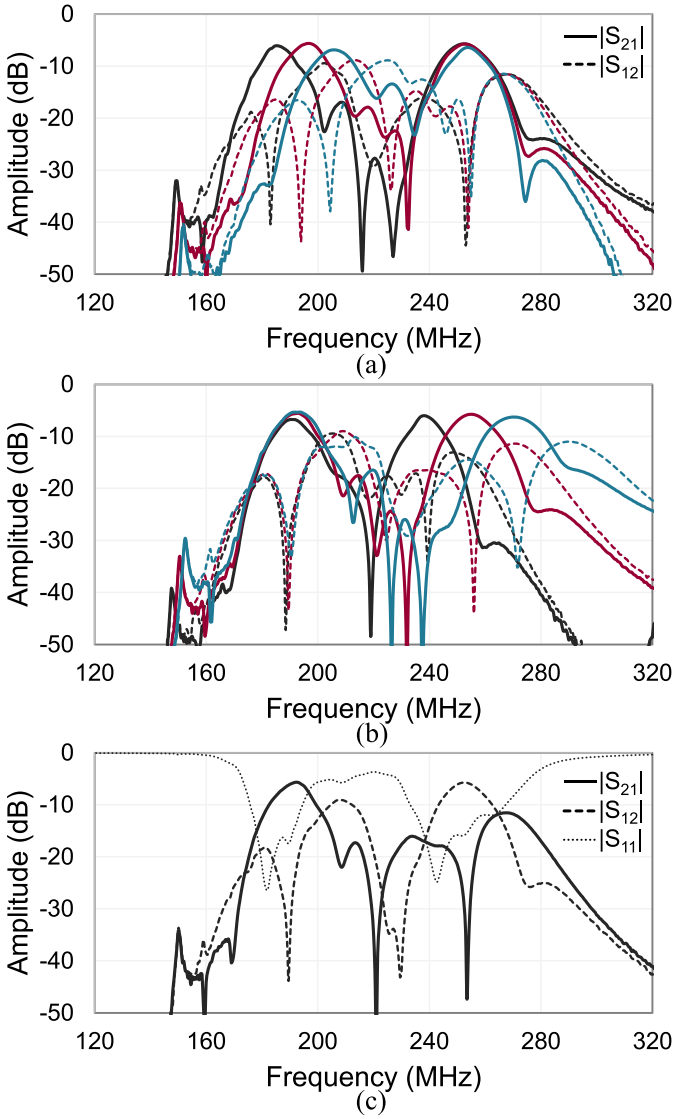

Fig. 21. RF measured power transmission and reflection responses of the manufactured circulator prototype in Fig. 19. (a) Tuning of the lower passband. (b) Tuning of the upper passband. (c) Reconfigurable directionality in the low- and in the high-frequency passband.

magnetless ones to date. Furthermore, the individual bands exhibit the second highest IS and are the only ones that achieve independent center frequency tuning, controllability of the number of active bands in the direction of propagation, and reconfigurability of the direction of propagation. The non-reciprocal filtering isolators in [10] and [11] only focus on single-band filtering configurations, and there is no mention of how to extend the single-band filters to multiband ones. Furthermore, the work in [10] is only tunable in frequency, and neither [10] or [11] demonstrates the tuning of the direction of propagation. Table II compares the magnetless circulator presented here with others in the state of the art. The circulator of this work is the only multiband, magnetless circulator to date. Moreover, it has the widest tuning range among all existing tunable magnetless circulators. In addition, it is the only magnetless circulator where the band center frequency tuning, the number of active bands in the direction

TABLE II
COMPARISON WITH STATE-OF-THE-ART FILTERING MAGNETLESS CIRCULATORS

Work	f_{cen}, MHz	BW, MHz (%)	IL, dB	In-band IS, dB	N	T
[6]	130	~15 (11.5)	~9	16-65	1	S
[12]*	500	~40 (8)	~4	19-32	2	S
[13]	825	130 (15.8)	1.7	10-27	2	S
[14]	1000	~100 (10)	3.4	14-28	1	S
[15]	970-1030 (1.06:1)	23 (2.3)	1.8	7-24	1	F
[16]*	1000	~30 (3)	2.9	11-47	1	S
This work	185-206 (1.11:1), 238-270 (1.13:1)	13.5 (6.9), 16.5 (6.5)	5.6, 5.5	14-50, 14-48.9	2, 2	F, D, B

*Simulations only, IS – isolation, N – branch order, T – tunability, S – static, F – frequency, D – direction of propagation, B – number of active bands

of propagation, and the reconfigurability of the direction of propagation can all be independently varied. Finally, it has among the highest IS with only [6] achieving a slightly higher IS.

IV. CONCLUSION

New classes of multiband, magnetless isolators and circulators with reconfigurable bandpass filtering capabilities have been presented in this manuscript. They are based on a transversal multipath BPF architecture where each path introduces a passband to the transfer function. Non-reciprocity is achieved by modulating the resonators of each path with progressively phase-shifted ac signals through varactor-based capacitances. The paths operate independently of each other, and so, the ac modulation parameters of each path can be separately determined and tailored for optimum RF performance. The operational principles of the magnetless isolator and circulator concept are demonstrated through various parametric studies and ideal simulations. It is shown that the STM imparted on the circuits' constituent varactor-based resonators results in high levels of IS and only one direction of signal propagation. The passbands can be independently tuned in center frequency by adjusting the dc biasing of the varactor diodes. Furthermore, by reversing the sign of the phase progression of the modulating ac signals, the direction of propagation can also be reconfigured. For proof-of-concept demonstration purposes, three LE prototypes, namely, dual- and three-band isolators and a dual-band circulator, were designed, manufactured, and measured. They exhibit the high in-band IS levels of up to 49.8 dB. All prototypes exhibit an independent band center frequency tuning of up to 1.22:1 and the ability to reconfigure the direction of propagation.

REFERENCES

[1] S. W. Y. Mung and W. S. Chan, "Active three-way circulator using transistor feedback network," *IEEE Microw. Wireless Compon. Lett.*, vol. 27, no. 5, pp. 476–478, May 2017.

[2] P.-H. Chen and R. M. Narayanan, "Design of active circulators using high-speed operational amplifiers," *IEEE Microw. Wireless Compon. Lett.*, vol. 20, no. 10, pp. 575–577, Oct. 2010.

[3] G. Hamoir, L. Piraux, and I. Huynen, "Control of microwave circulation using unbiased ferromagnetic nanowires arrays," *IEEE Trans. Magn.*, vol. 49, no. 7, pp. 4261–4264, Jul. 2013.

[4] N. Reiskarimian and H. Krishnaswamy, "Fully-integrated non-magnetic non-reciprocal components based on linear periodically-time-varying circuits," in *Proc. IEEE 17th Topical Meeting Silicon Monolithic Integr. Circuits RF Syst. (SiRF)*, Jan. 2017, pp. 111–114.

[5] A. Kord, D. L. Sounas, and A. Alu, "Differential magnetless circulator using modulated bandstop filters," in *IEEE MTT-S Int. Microw. Symp. Dig.*, Jun. 2017, pp. 384–387.

[6] N. A. Estep, D. L. Sounas, and A. Alu, "Magnetless microwave circulators based on spatiotemporally modulated rings of coupled resonators," *IEEE Trans. Microw. Theory Techn.*, vol. 64, no. 2, pp. 502–518, Feb. 2016.

[7] X. Wu et al., "Isolating bandpass filters using time-modulated resonators," *IEEE Trans. Microw. Theory Techn.*, vol. 67, no. 6, pp. 2331–2345, Apr. 2019.

[8] X. Wu, M. Nafe, A. A. Melcon, J. S. Gomez-Diaz, and X. Liu, "A non-reciprocal microstrip bandpass filter based on spatio–temporal modulation," in *IEEE MTT-S Int. Microw. Symp. Dig.*, Jun. 2019, pp. 9–12.

[9] X. Wu, M. Nafe, A. Melcón, J. S. Gomez-Diaz, and X. Liu, "Frequency tunable non-reciprocal bandpass filter using time-modulated microstrip $\lambda_g/2$ resonators," *IEEE Trans. Circuits Syst. II, Exp. Briefs*, vol. 68, no. 2, pp. 667–671, Feb. 2021.

[10] D. Simpson and D. Psychogiou, "Magnet-less non-reciprocal bandpass filters with tunable center frequency," in *Proc. 49th Eur. Microw. Conf. (EuMC)*, Oct. 2019, pp. 460–463.

[11] D. Simpson and D. Psychogiou, "Fully-reconfigurable non-reciprocal bandpass filters," in *IEEE MTT-S Int. Microw. Symp. Dig.*, Aug. 2020, pp. 807–810.

[12] M. Nafe, X. Wu, and X. Liu, "A wideband magnetic-free circulator using spatio–temporal modulation of 2-pole bandpass filters," in *Proc. IEEE Radio Wireless Symp. (RWS)*, Jan. 2019, pp. 1–3.

[13] X. Wu, M. Nafe, and X. Liu, "A magnetless microstrip filtering circulator based on coupled static and time-modulated resonators," in *IEEE MTT-S Int. Microw. Symp. Dig.*, Aug. 2020, pp. 948–951.

[14] X. Wu and X. Liu, "A magnetless 4-port circulator and its microstrip implementation," *IEEE Trans. Circuits Syst. II, Exp. Briefs*, vol. 69, no. 3, pp. 969–973, Mar. 2022.

[15] A. Kord, D. L. Sounas, and A. Alù, "Pseudo-linear time-invariant magnetless circulators based on differential spatiotemporal modulation of resonant junctions," *IEEE Trans. Microw. Theory Techn.*, vol. 66, no. 6, pp. 2731–2745, Jun. 2018.

[16] M. Nafe, M. N. Hasan, H. Reggad, D. Kuzmenko, J. Chen, and X. Liu, "Magnetic-free circulator based on spatio–temporal modulation implemented via switched capacitors for full duplex communication," in *Proc. USNC-URSI Radio Sci. Meeting (Joint With AP-S Symp.)*, Jul. 2018, pp. 119–120.

[17] S. Cheab, P. W. Wong, and S. Soeung, "Design of multi-band filters using parallel connected topology," *Radioengineering*, vol. 27, no. 1, pp. 186–192, Apr. 2018.

[18] E. Guerrero, J. Verdu, and P. D. Paco, "A synthesis view to dual-band responses with parallel-connected acoustic wave filters," in *Proc. IEEE 21st Annu. Wireless Microw. Technol. Conf. (WAMICON)*, Apr. 2021, pp. 1–4.

[19] G. Macchiarella and S. Tamiazzo, "Dual-band filters for base station multi-band combiners," in *IEEE MTT-S Int. Microw. Symp. Dig.*, Jun. 2007, pp. 1289–1292.

[20] H. Meng and K.-L. Wu, "Direct optimal synthesis of microwave dual band filters with parallel-connected topology," in *IEEE MTT-S Int. Microw. Symp. Dig.*, May 2016, pp. 1–4.

[21] G. Macchiarella and S. Tamiazzo, "Synthesis of dual-band filters with parallel-connected networks," in *Proc. 44th Eur. Microw. Conf.*, Oct. 2014, pp. 608–611.

[22] C.-Y. Chen and C.-Y. Hsu, "A simple and effective method for microstrip dual-band filters design," *IEEE Microw. Wireless Compon. Lett.*, vol. 16, no. 5, pp. 246–248, May 2006.

[23] D. M. Pozar, *Microwave Engineering*, 4th ed. Hoboken, NJ, USA: Wiley, 2012.

Dakotah Simpson (Member, IEEE) received the B.S. degree in electrical engineering from the South Dakota School of Mines and Technology, Rapid City, SD, USA, in 2017, and the M.S. degree in electrical engineering from the University of Colorado Boulder, Boulder, CO, USA, in 2020, where he is currently pursuing the Ph.D. degree in electrical engineering.

His current research interests include the design, characterization, and synthesis of reconfigurable RF/microwave single-ended and balanced filters and frequency selective feed networks for linear antenna arrays.

Prof. Simpson is a member of the IEEE Microwave Theory and Techniques Society (IEEE MTT-S) and the Applied Computational Electromagnetics Society (ACES). He was a recipient of the MTT-S 2018 Graduate Fellowship, the University of Colorado's Dean's Graduate Assistantship and the electrical, computer, and energy engineering (ECEE) Gold Award for Research, and the 2018–2019 Lockheed Martin Endowed Graduate Fellowship. He received the first-place prize at the 2018 International Microwave Symposium (IMS) Student Design Competition and the 2018 European Microwave Week (EuMW) Student Design Competition and the second-place prize at the 2019 IMS Student Design Competition.

Dimitra Psychogiou (Senior Member, IEEE) received the Dipl.-Eng. degree in electrical and computer engineering from the University of Patras, Patras, Greece, in 2008, and the Ph.D. degree in electrical engineering from the Swiss Federal Institute of Technology (ETH), Zürich, Switzerland, in 2013.

She was a Senior Research Scientist with Purdue University, West Lafayette, IN, USA, and an Assistant Professor with the University of Colorado Boulder (UC Boulder), Boulder, CO, USA. She is currently a Professor of electrical and electronic engineering with the University College Cork (UCC), Cork, Ireland, and the Tyndall National Institute, Cork. Her current research interests include the RF design and characterization of reconfigurable microwave and millimeter-wave passive components, acoustic wave resonator-based filters, tunable filter synthesis, and additive manufacturing techniques for antennas and RF front-end components.

Prof. Psychogiou is a Senior Member of International Union of Radio Science (URSI) and a member of the IEEE Microwave Theory and Techniques Society (IEEE MTT-S) Filters and Passive Components (MTT-5) and Microwave Control Materials and Devices (MTT-13) Committees. Her research has led to 200 publications and has received the 2021 Roberto Sorrentino Prize from the European Microwave Association (EuMA), the 2021 Research Professorship Award from the Science Foundation Ireland (SFI), the 2020 CAREER Award from the National Science Foundation (NSF), USA, the 2020 URSI Young Scientist Award, and the Junior Faculty Outstanding Research Award from UC Boulder. She is the Chair of MMT-13 and the Secretary of the United States National Committee (USNC)-URSI Commission D. She serves on the Technical Review Board for various IEEE and EuMA conferences and journals. She was an Associate Editor of the *IET Microwaves, Antennas and Propagation Journal*. She is an Associate Editor of the IEEE MICROWAVE AND WIRELESS COMPONENTS LETTERS and the *International Journal of Microwave and Wireless Technologies*.